Study on the carbon nanotubes reinforced nanocomposite coatings

Ji, Xiaochao; Li, Xiaoying; Yu, Helong; Zhang, Wei; Dong, Hanshan

DOI:
10.1016/j.diamond.2018.11.027

Document Version
Peer reviewed version

Citation for published version (Harvard):
Ji, X, Li, X, Yu, H, Zhang, W & Dong, H 2019, 'Study on the carbon nanotubes reinforced nanocomposite coatings', *Diamond and Related Materials*, vol. 91, pp. 247-254. https://doi.org/10.1016/j.diamond.2018.11.027

Study on the carbon nanotubes reinforced nanocomposite coatings

Xiaochao Ji[a,b], Xiaoying Li[a], Helong Yu[b], Wei Zhang[c], Hanshan Dong[a]

[a]*School of Metallurgy and Materials, The University of Birmingham, Birmingham B15 2TT, UK*

[b]*National Key Laboratory for Remanufacturing, AAFE, Beijing 100072, China.*

[c]*Jingjinji Institute of Remanufacturing Industry & Technology, Hebei 062450, China*

Abstract: One-dimensional nanocomposite coatings are a new generation of coatings, which have promising applications in versatile fields. In this study, the novel carbon nanotubes (CNTs) reinforced nanocomposite coatings were explored through two-step strategy using both physical vapour deposition (PVD) approach and chemical vapour deposition (CVD) approach. Vertically aligned CNT films were deposited by plasma enhanced CVD at 450□, while density of the VACNT films was modified by using Ag impregnated composite catalyst films. Subsequently, Pt-CNT, Ag-CNT and DLC-CNT nanocomposite coatings were explored to find a feasible way to achieve the well-designed composite structure. Morphologies and microstructures of these nanostructures were characterized by scanning electron microscopy, atomic force microscopy, transmission electron microscopy and Raman spectroscopy, while four-probe tester was applied to evaluate the electrical conductivity of the nanocomposite coatings. The results indicated that well-composited DLC-CNT nanocomposite coating can be achieved which exhibited better electrical conductivity compare to that of the pristine DLC coating.

Keywords: carbon nanotubes, nanocomposite coating, diamond like carbon, wettability, electrical conductivity, PECVD

1. Introduction

Nanocomposite coatings are a new category of coatings which may have unique mechanical, physical and multifunctional properties which have shown increasing interest in industries, such as automotive, electronics and aerospace [1]. Composite structures are promising for addressing the limitations of conventional monolithic structures to achieve excellent combination of strength, stiffness, toughness, and some other functional properties [2]. Compare to bulk composite materials, which can be classified based on the dimension of the reinforcements, structures of nanocomposite coatings also can be similarly grouped into dimension by reinforcements, such as the zero-dimensional multicomponent coatings [3, 4], one-dimensional nanofiber reinforced coatings [5-7], two-dimensional multilayer coatings [8, 9], and three-dimensional multigrain coatings [10].

Nanofibers are widely used as reinforcements in bulk polymers, ceramics, and metals based composite materials [11-13]. However, less studies have been carried out to fabricate the one-dimensional nanocomposite coatings, which may have excellent properties due to the unique microstructures of the nanofibers. Thus, it is important to explore feasible approaches for the deposition of nanofibers reinforced composite coatings. Carbon nanotube (CNT) is one of the most attractive one-dimensional materials which has high aspect ratio, enhanced tensile and elastic properties, excellent electrical and thermal conductivity, etc. [14]. These extraordinary properties make CNTs one of the most promising reinforcements for the one-dimensional nanocomposite coatings, to improve the tribological, corrosion, electronical or thermal properties of the coating system [15-18].

In fact, the overall performances of the CNTs reinforced composite coatings are determined by the distribution of the reinforcements in the matrix [19]. However, it is difficult to achieve a homogeneous dispersion of the CNTs because of agglomeration. Researchers have developed different strategies to fabricate the CNTs reinforced nanocomposite coatings, including the premixing process and two-step approach.

The premixing process is commonly utilized for wet deposition processes, such as electrodeposition [20-24], electroless plating [25, 26], electro-brush plating [27]. Guo et al. fabricated the CNTs reinforced Ni based nanocomposite coating using the electrodeposition process, while the existence of CNTs can improve strength, toughness, and corrosion resistance of the composite coating [20, 21]. Akyol et al. deposited a CNTs reinforced Ni-W-P composite coating by electroless deposition which exhibited enhanced hardness and corrosion resistance [26]. The Fe/CNTs composite coating showed low friction coefficients and wear resistance due to the lubrication effect of CNTs which was fabricated by electro-brush plating [27]. However, the ultrasound agitation and stirring cannot totally avoid the aggregation of CNTs in wet environment. Therefore, it was considered that appropriate dispersants are needed to avoid the re-aggregation of CNTs in the plating bath, and the results indicated that mechanical atomization yielded best effective at disintegration compared to magnetic stirring and ultrasonic homogenization [25].

Premixing methods like ball milling and *in-situ* preparation are also feasible for thermal spray coating deposition processes, which are conventionally used for bulk composites depositions [28]. CNTs reinforced Al [29], Cu [30], and TiO_2 [31] based nanocomposite coatings have been developed in the past decades, Bakshi et al. prepared the CNTs reinforced Al nanocomposite coating by cold spray, and elevated elastic modulus was achieved when 0.5 wt. % CNTs were loaded [29]. However, it

was reported that the mechanical mixing process can cause damage to the CNTs to some extent [32]. Besides, CNTs/metal particles were *in-situ* formed by CVD methods in order to achieve a homogeneous distribution of CNTs [33, 34]. Conversely, the harsh growth conditions may cause degradation to the metal particles [33].

The premixing approach provides a practical way to achieve the randomly dispersed CNTs reinforced nanocomposite coatings, which is concentrated on the improvement on the mechanical properties of the nanocomposite coatings. The two-step strategies intend to use the vertically aligned CNT (VACNT) films as base for the deposition of multifunctional nanocomposite coatings [5], due to the unique properties of the vertically aligned architecture, which can avoid the damage on CNTs through the premixing process. However, limited studies have been conducted using the two-step approach due to the challenge to diffuse the matrix into the high density VACNT films.

Kinoshita et al. developed the CNTs reinforced DLC nanocomposite coatings with microwave PECVD. Nevertheless, the DLC matrix cannot fully infiltrate into the dense VACNT films, even though the internal stress of the composite coating was decreased [5]. Jampani et al. prepared 3D architecture of VO_x/VACNT through the two-step approach, vanadium oxides were deposited on the CNTs by CVD process. As considered that the composite structures have a lot of advantages, such as high electronic contact, good ballistic electron transport, short diffusion distance from interface to interface, and high overall capacitance [35]. Zanin et al. studied the field emission property of the DLC-CNT hybrid which exhibited high emission current, great stability, and long lifetime [36]. Susantyoko et al. sputtered to form the NiO/VACNT composite electrode for lithium ion batteries, while significantly

improvement in capacity was achieved due to the composite structure which can provide superior ion and electron transport [37]. Consequently, it was considered that the organised architectures can provide multifunctional properties to the nanocomposite coatings [38-40]. However, there is a general shortcoming in achieving these composite structures, because the dense VACNT film will limit the infiltration of the matrix. Thus, it is timely from both scientific and practical view-point to develop feasible approach to form well-designed VACNTs reinforced nanocomposite coatings.

In this work, the VACNTs reinforced nanocomposite coatings were fabricated using the atomic deposition processes in order to get a fully composited architecture. VACNT films were grown by PECVD, while inert element contained catalyst films were applied to decrease the density of the VACNT films. Furthermore, both physical vapour deposition and chemical vapour deposition methods were utilized to fill the matrix into the intertube gaps between the CNTs. Morphologies and microstructures of these nanocomposite coatings were characterized by SEM, AFM, TEM, and Raman spectroscopy, and the formation mechanisms of the nanocomposite coatings are summarised based on these results. Electrical conductivity was measured by a four-probe tester to evaluate the performances of these nanocomposite coatings. These one-dimensional nanofibers reinforced composite structures could be used to improve electrical, tribological or thermal properties of the composite coatings.

2. Experimental

Silicon wafers (100) (Lijing Ltd. China) were used as substrates. Stainless-steel (SS) and Ag-SS catalyst films were deposited by the novel active screen plasma (ASP) technique using a DC Klöckner Ionon 40 kW furnace. The sputtering processes were

carried in an ambient of hydrogen plasma at 200□ for 10 min using different lids. Vertically aligned CNTs were subsequently synthesized at 450□ for 100 min by a commercial rf PECVD (P500, 13.56MHz, Thin Film Solution Ltd). The growth processes were conducted at 30 W and acetylene was used as carbon source, diluted by argon and hydrogen, and their corresponding flow rate were 5 sccm, 50 sccm and 10 sccm. The specific settings are shown in our previous work [41]. The VACNT films were used as substrates for the fabrication of the nanocomposite coatings. Pt-CNT coatings were deposited with a mini sputter coater with Pt target at room temperature for 3 min. Ag-CNT coatings were fabricated with a magnetron sputtering (Teer Coatings Ltd) for 10 min with a pure silver target. DLC-CNT films were deposited by the rf PECVD at 170□ for 30 min and methane (10 sccm) was used as carbon source.

Morphologies of catalyst films, VACNT films and their cross-sections were observed by scanning electron microscopy (SEM, JEOL 7000). The multimode AFM (Veeco, Digital Instruments) was applied to investigate the surface morphologies of the nanocomposite coatings while contact mode was applied during the measurements. Transmission electron microscope (TEM, Oxford JEOL 2100 LaB_6) coupled with energy-dispersive X-ray spectroscopy (EDS) was employed to analyse nanostructure and composition of the CNTs, while all analyses were carried out at an acceleration voltage of 200 kV. TEM specimens were prepared by dispersing CNTs onto a holey carbon film supported by a Cu grid.

Raman spectra of the VACNTs and the related nanocomposite coatings were measured at room temperature using a Renishaw inVia Raman Microscopy with excitation of 488nm. Biolin Scientific Theta contact angle meter was applied to investigate the wettability of the samples, while distilled water (γ_{tot} = 72.8 mN m^{-1}, γ_d

= 21.8 mN m^{-1}) was used as droplets and the dropout volume was around 2.5 μl with a dropout rate of 0.5 μl/s, whilst the contact angles were measured by the software. Electrical conductivities of the nanocomposite coatings were evaluated by an RTS-8 four-point probe apparatus, while a current source was applied on two of the probes, and the inducing voltage on the other two probes were measured to calculate the sheet resistances.

3. Results and discussion

3.1 Catalyst films

Surface morphologies of the catalyst films are shown in Figure 1. The catalyst films were formed by the nanoparticles sputtered from the active screen lids. Figure 1(a) shows the SS catalyst film, sizes of these SS nanoparticles are around 20 nm, and the nanoparticles are uniformly distributed on the surface. Figure 1(b) shows the morphologies of the Ag-SS catalyst film. Unlike the SS catalyst film, some large particles are randomly distributed on the surface, which were verified to be Ag particles, attributing to the high sputter rate of silver [42]. Sizes of these Ag particles varied from ~10 nm to ~500 nm. It is known that noble silver does not have catalytic function for the growth of CNTs, because the solubility of graphitic carbon in silver is limited and cannot form stable carbides [43]. Thus, these silver particles can act as barriers in prohibiting of the growth CNTs in order to decrease the density of the VACNT films. The using of composite catalyst film provide a more convenient way to control density of the VACNT films, compare to other potential methods, such as patterning [44] and other post treatments [45].

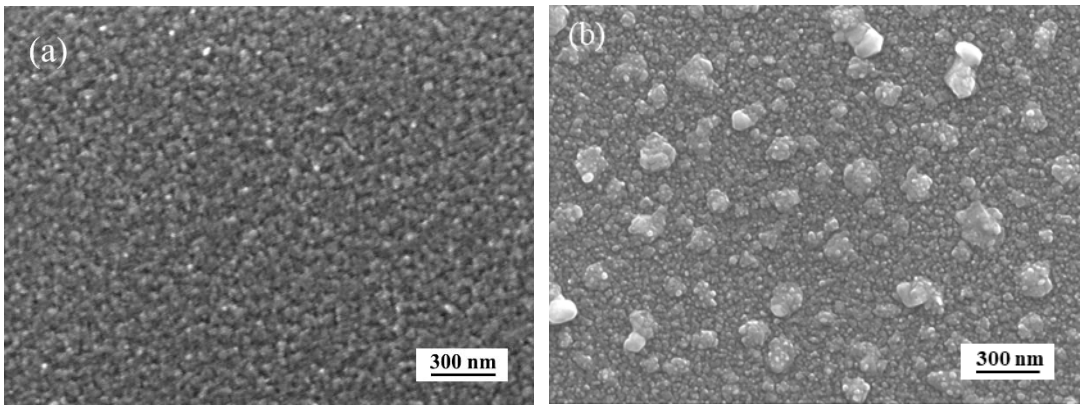

Figure 1 Catalyst films deposited by active screen plasma technique: (a) SS catalyst film; (b) Ag-SS catalyst film with large Ag particles on the surface.

3.2 VACNT films

Figure 2 exhibit the surface and cross-section morphologies of the as-deposited CNTs films. CNTs films grown from the SS catalyst films are shown in Figure 2 (a) & (b), while a high density ($10^{11}/cm^2$) of CNTs was achieved which makes it difficult for the matrix to diffuse into the film. Vertically aligned structure of the CNTs can be viewed in Figure 2 (b). It is attributed to the Van der Waals forces between these CNTs that drive the align growth of CNTs [46]. The length and diameter of the as grown CNTs are around 1 μm and 30 nm, respectively.

Figure 2 (c) & (d) present the VACNT films synthesized from the Ag-SS catalyst film. Beside the CNTs, some silver particles also can be viewed embedded in the film. Density of the CNTs is around $10^9/cm^2$ which is lower compared to that grown from the SS catalyst films. The cross-section view in Figure 2 (d) shows that CNTs grown from the Ag-SS catalyst film are relatively curly due to the gaps between the CNTs. This verified that noble Ag particles were effective to inhibit the growth of CNTs, which is a feasible way to control the density of the VACNT film.

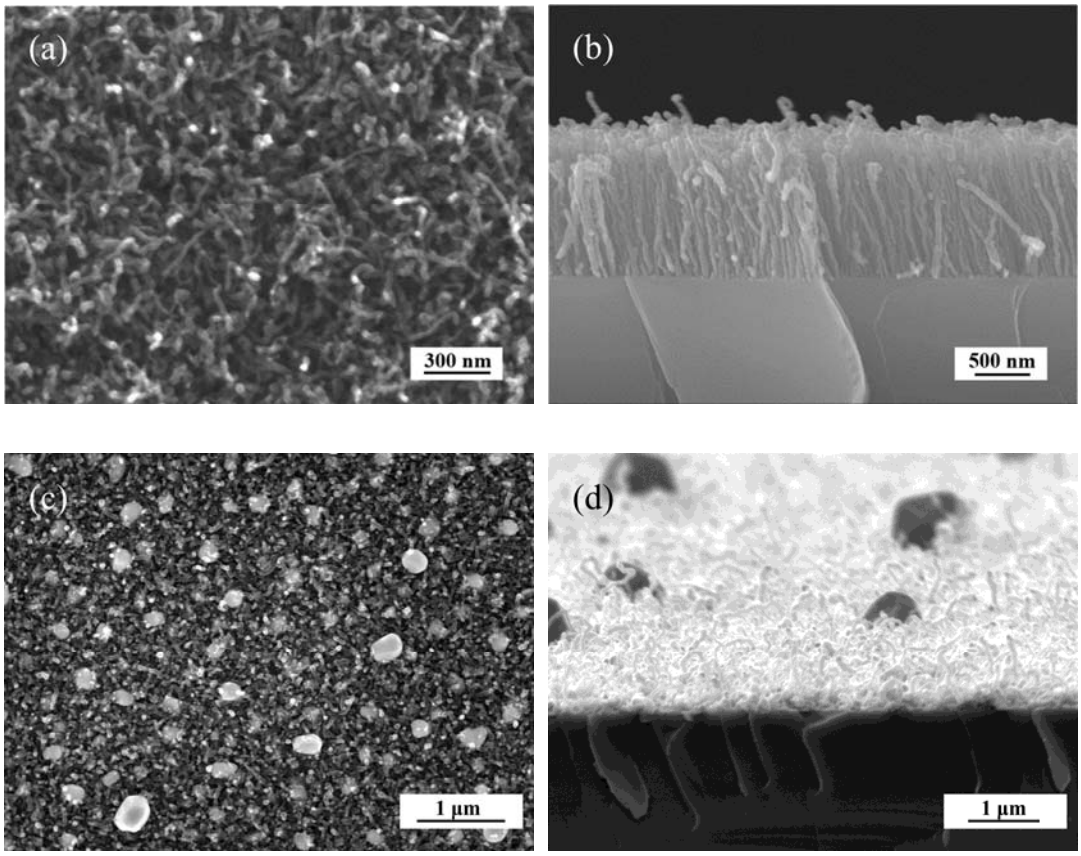

Figure 2 SEM images the CNT films grown from SS catalyst film ((a), (b)) and Ag-SS catalyst film ((c), (d)).

TEM was applied to investigate the microstructures of the as-deposited CNTs. Figure 3(a) shows the CNTs grown from the SS catalyst film, while tubular structure of the CNTs can be distinguished and metal particles were embedded at tip of the CNTs which were verified to be SS nanoparticles, indicating a tip growth mode is applicable to explain the formation of the CNTs. Diameters of the as-grown CNTs are ranged between 10 nm to 50 nm and the average diameter is 23 nm. The length-diameter ratio is around 50 which makes them suitable as reinforcements. Figure 3(b) shows the CNTs grown from the Ag-SS catalyst which have an average diameter of 28 nm. The nanoparticles embedded in the tips of the CNTs suggested that these CNTs were also

formed with a tip growth mechanism. However, beside these multi-walled CNTs, some carbon nanofibers (CNFs) were also generated from the Ag-SS catalyst film. As no catalyst particles are found in the CNFs, indicating these CNFs were formed with a bottom growth mechanism.

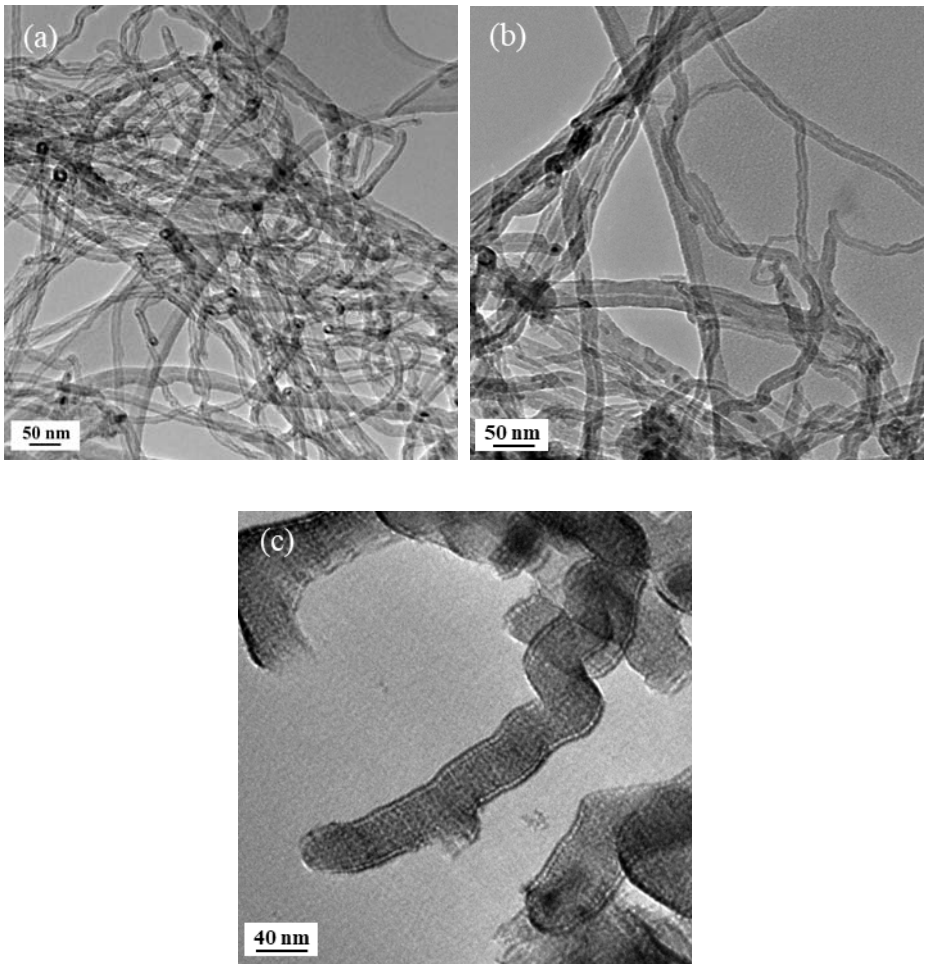

Figure 3 TEM images of CNTs: (a) CNTs grown from SS catalyst film; (b) CNTs grown from Ag-SS catalyst film; (c) CNFs grown from Ag-SS catalyst film.

Raman spectra of the CNTs grown from both types of catalyst films are shown in Figure 4. Obvious Raman features were detected from both VACNT films, beside the typical D band and G band at around 1350 cm^{-1} and 1600 cm^{-1}, peaks belong to 2D band and D+G band were also detected, indicating that the as-grown CNTs have multi-walled structures [47].

It is known that Raman features of CNTs are detected from the vibrations of the carbon atoms, while the D band comes from a double resonance process and G band is assigned to the in-plane vibration of C-C bonds [48]. Thus, the microstructures of CNTs can influence the position and intensity of the D band and G band. Raman shifts of D band and G band of the CNTs grown from SS catalyst films are at 1337 cm^{-1} and 1608 cm^{-1} respectively. The corresponding features of the CNTs synthesized from the Ag-SS catalyst films are closer to each other, which are at 1360 cm^{-1} and 1598 cm^{-1}, due to the formation different carbon nanofibers. Whilst the D band to G band intensity ratio (I_D/I_G) of these two CNT films are 0.71 and 0.85, respectively. Higher intensity ratio of the CNTs grown from Ag-SS catalyst film indicates more defects were generated within the CNTs, which may cause by the interference of silver particles.

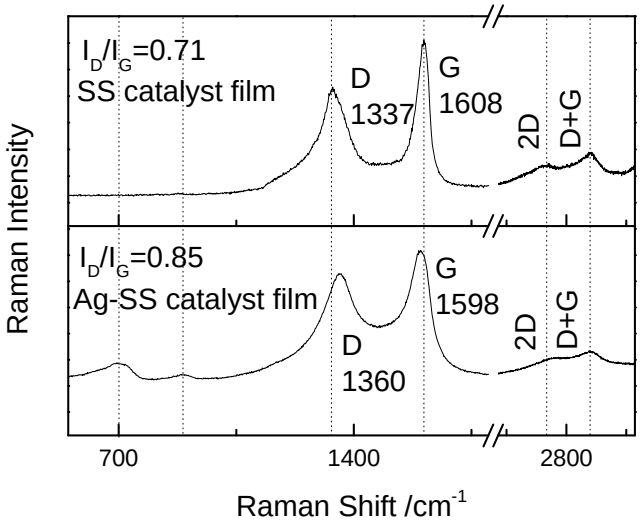

Figure 4 Raman spectra of the VACNT films grown from stainless steel catalyst film and Ag impregnated stainless steel catalyst film.

3.3 Nanocomposite coatings

Several attempts have been carried out to explore the deposition of the CNTs reinforced nanocomposite coatings through the two-step approach. VACNT films

with different density were applied to find an applicable method to achieve the well-designed composite structure.

Figure 5 (a) presents surface morphology of the Pt-CNT nanocomposite coating, and there was no dense composite structure formed due to the low sputter rate of Pt. Pt nanoparticles were generated during the sputtering process, which are feasible to penetrate through the CNT film, and coated on the CNT surface. However, the continuous impacts from the Pt nanoparticles can break the vertically aligned structure of the CNTs. The insert TEM image illustrates that Pt nanoparticles were coated on the wall of CNT with size of about 5 nm. It is difficult for the small Pt nanoparticles to fully fill the gaps without damaging the VACNT films.

Sizes of the sputtered particles are correlated with the sputtering conditions and the intrinsic property of the targets during a PVD process. Figure 5 (b) shows the cross-section view of the Ag-CNT nanocomposite coating, while large silver particles were formed during the sputtering process, which cannot infiltrate into the CNT film, whilst an obvious interface between the Ag layer and the CNT layer can be observed. Mechanical bonds were formed due to the impact effects from the Ag particles.

Due to the impact effects, CNTs in a low density VACNT film are vulnerable, which can be damaged by the particles in a PVD process. Thus, PVD approach is not capable to fabricate a well-designed composite coating even with a low-density CNT film. However, the multilayer composite structures can be recognised as 2D composite coating, which also have some potential applications [37].

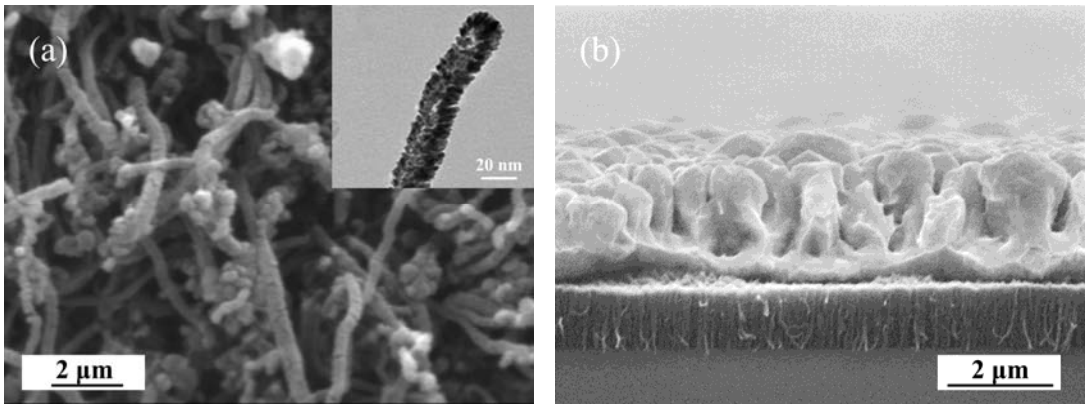

Figure 5 SEM images of the CNTs reinforced nanocomposite coatings deposited by PVD method: (a) Pt-CNT composite coating; (b) Ag-CNT composite coating.

Unlike the sputtering process, volatile precursors in the CVD process can easily diffuse into the CNT film and coat on the CNTs, while amorphous carbon was used as matrix in the CVD process. Figure 6(a) shows that a surface amorphous carbon layer is coated on top of the dense VACNT film, and it has found that the matrix preferred to accumulate on the tips of the CNTs, and the accumulation layer will inhibit the continuous diffusion of the amorphous carbon matrix. Surface morphology of the nanocomposite coating is shown in Figure 6(c), while granular surface was formed with a roughness around 13.2 nm, due to the aggregation of amorphous carbon on the CNT tips. Chemical bonds were formed between the amorphous carbon and the CNTs, whilst better adhesion can be achieved compare to the PVD composite coatings.

To improve the diffusion of the amorphous carbon, low density VACNT films were deposited using the Ag-SS catalyst films. The cross-section image of the DLC-CNT nanocomposite coating is shown in Figure 6(b), while the amorphous carbon was fully diffused into the VACNT film, revealing that well-composited structure can be formed with the low density VACNT film. A relatively smaller surface roughness was obtained of the well-designed DLC-CNT nanocomposite coating, which are about 6.8

nm, and the surface morphology of this coating is exhibited in Figure 6(d) which has a mild surface.

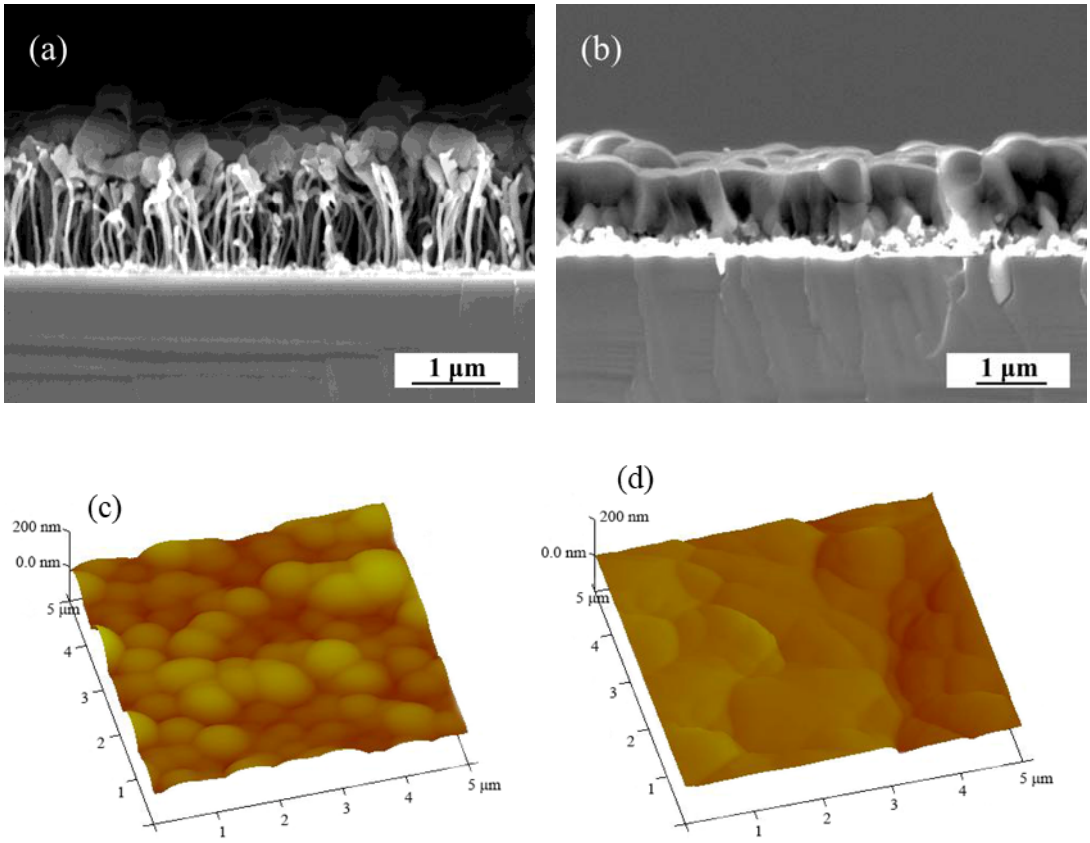

Figure 6 SEM images of the CNTs reinforced composite coatings: (a) DLC-CNT grown from high-density CNT film; (b) DLC-CNT grew from low-density CNT film. (c) AFM surface morphology of (a); (d) AFM surface morphology of (b).

Raman spectra comparison between the DLC film, the CNT film and the DLC-CNT nanocomposite coating are shown in Figure 7. The DLC coating exhibited overlapped D band and G band due to its amorphous structure and its intensity ratio is 0.58, while separated D band and G band were achieved from the multiwalled CNTs and the intensity ratio is 0.85. For the DLC-CNT composite coating, its Raman spectrum is a combination of the amorphous carbon and the CNTs and its intensity ratio is 0.71. Even though the amorphous carbon layer is the outside layer, but the Raman features from the CNTs are in dominant.

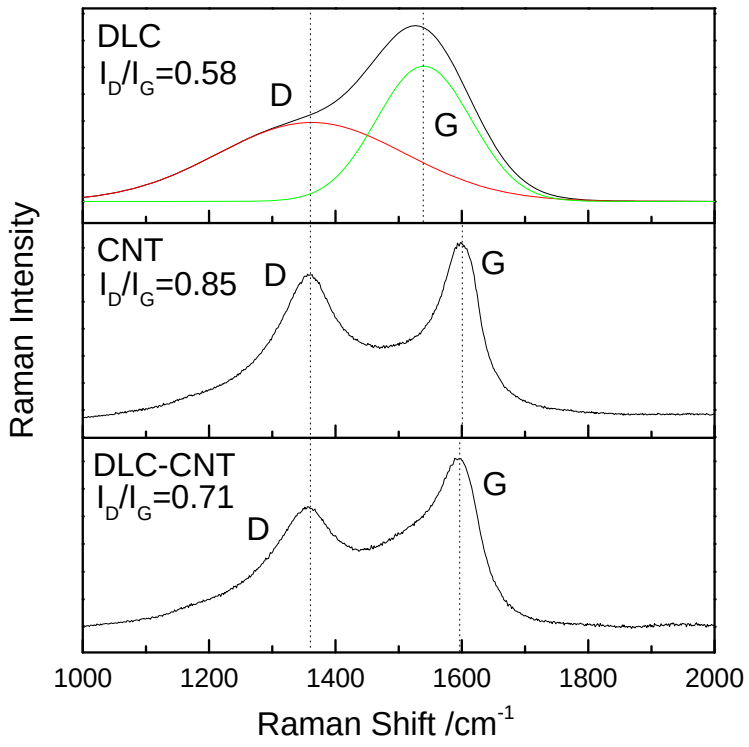

Figure 7 Comparison of the Raman spectra between DLC film and VACNT film grown from Ag-SS and DLC-CNT composite coating grown from the low-density CNT film.

3.4 Formation mechanisms

Schematic diagrams of three typical composite structures are shown in Figure 8. PVD process is applicable to fabricate the double layers structure (Figure 8(a)), because the sputtered particles with high kinetic energy can be supported with the dense VACNT film. This composite structure is capable to be used as electrode for lithium-ion batteries [37], because the CNT array is an excellent current collector, which exhibit low internal resistance and low charge transfer resistance.

In a CVD process, the volatile precursors are feasible to diffuse into gaps between the aligned CNTs. However, the interactions between the nanofiber reinforcements and the matrix are complex, while the matrix can accumulate on the tips of the nanofibers to form the composite structure as shown in Figure 8(b). More defects could be generated which is useful to improve the electrical conductivity of nanocomposite

coating and benefit the application of this type of nanocomposite coating in energy storage due to the active sites [49].

To acquire the well-designed nanocomposite structure shows in Figure 8(c), low-density nanofiber films are needed which is benefit for the diffusion of the volatile precursors. Several ways were reported to control the density of the CNT films by modifying the catalyst films, such as patterning by electron beam lithography or photolithography [50, 51], size control of the catalyst particles, or composition adjustment of the catalyst film [52, 53]. The composite catalyst film applied in this study is a convenient and cost-effective way to control the density of the VACNT film. However, due to the high sputter rate of Ag, some large Ag particles were formed during the sputtering process which may affect the performance of the composite coating. Other elements like Cu or Ti should be explored to have a better control of the catalyst film. The ideal status of the 1D nanocomposite coating should equip with the properties both from the matrix and the reinforcements. Further studies are required to create a controllable approach for the formation of the well-designed 1D nanocomposite structure.

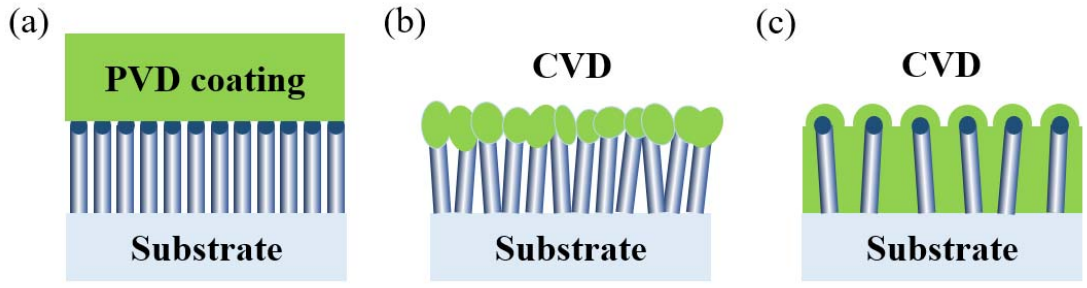

Figure 8 Schematic images of the typical composite structures deposited by PVD and CVD approaches. (a) PVD coating accumulated on the surface of the VACNT film; (b) CVD coating accumulated on the tips of the CNTs; (c) CVD coating infiltrated inside the VACNT film to form the well-designed nanocomposite coating.

3.5 Wettability and roughness

Wettability is used to evaluate the interactions between a surface and a liquid. It is known that VACNT is superhydrophobic due to its nanostructure. In this study, the composite surface was influenced by the bottom VACNT film. Besides, wettability of the composite surface can affect the interactions between the composite surface and counterparts in wet conditions. Wettability of the CNT related coatings were investigated which are shown in Figure 9. Variation of the contact angles are mainly influenced by the morphologies and chemical status of the coatings. In this case, these amorphous carbon surfaces have similar chemical status. Thus, their wettability is mainly affected by surface roughness. The pure DLC coating is very flat with a roughness of 4 nm and the contact angle is around 91^{o}. For the DLC-CNT composite coating deposited from the high density VACNT films, a relative rough surface (~13.2 nm) was formed because the amorphous carbon was mainly attached to the tips of the CNTs and resulted in a higher contact angle of 145^{o}. The amorphous carbon can fully diffuse into the gap of the low density VACNT film to form a composite coating with lower roughness (~6.8 nm) and its contact angle is around 115^{o}.

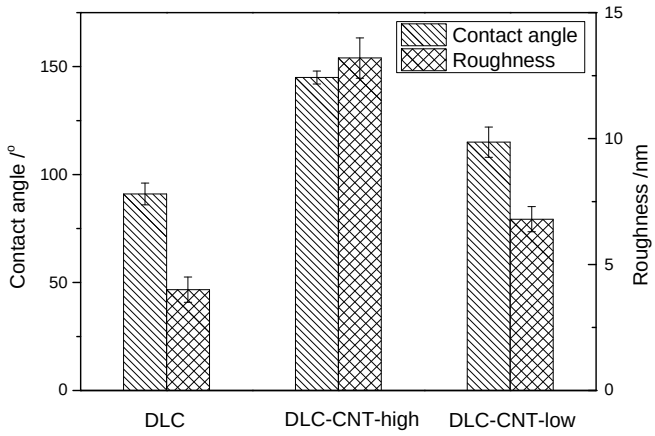

Figure 9 Contact angle and surface roughness of the DLC coating, the DLC-CNT coating deposited from high density VACNT film, and the DLC-CNT coating deposited from low density VACNT film.

3.6 Electrical conductivity

Electrical conductivity of the as-deposited composite coatings was measured by a four-probe tester with 1 mm probe distance. CNTs are known for their high electrical property along the axis of the nanotube which had been spin together as low-resistance electrical wires [54]. However, the electrical conductivity of the VACNT film is also affected by the vacancies between the CNTs. It is revealed that the VACNT films grown from the SS catalyst film presented a sheet resistance of 8.36 $k\Omega sq^{-1}$, which is much higher compared to that of the VACNT film grown from the Ag-SS catalyst film (135 Ωsq^{-1}). This is because Ag particles embedded in the VACNT film also equipped with high electrical conductivity, and the catalyst layer was helpful to decrease the overall sheet resistance of the film.

It was measured that the amorphous carbon film was nonconductive due to the disordered carbon within the film. However, the DLC-CNT nanocomposite coatings were verified to be conductive though relatively high sheet resistances were measured. The sheet resistances of the DLC-CNT-high and the DLC-CNT-low nanocomposite coatings are about 212.6 $k\Omega sq^{-1}$ and 623.5 $k\Omega sq^{-1}$ respectively. The DLC-CNT-low composite coating presents a higher sheet resistance because the amorphous carbon was well infiltrated to form a denser composite structure with less voids and defects. The conductivity of the nanocomposite coating can be attributed to the defects within the coatings, whilst the embedded CNTs can provide channels for the transfer of electrons.

4. Conclusions

This article has provided a deeper insight into the formation of the CNTs reinforced nanocomposite coating, while the two-step strategy was applied to build up the composite structures based on the VACNT films. Novel ASP technique was utilized to prepare the SS and Ag-SS catalyst films in order to control the growth of CNTs. It was proved that well-designed DLC-CNT nanocomposite coating can be achieved using the low-density VACNT film through the CVD approach, which had a dense structure and conductive. Besides, the double layer structures can be formed with the high-density VACNT film using both PVD and CVD process, because the dense CNT array can prohibit the continuous infiltration of the matrix. These nanocomposite structures may offer highly diverse properties due to their unique structures, which can be used as electrodes, biosensors, etc.

Acknowledgement

The authors wish to express their appreciation to the financial support of the EC FIBRALSPEC project (Grant No. 604248), EC H2020-MODCOMP project (Grant No. GA685844) and National Key R&D Program of China (2017YFB0310703, 2017YFF0207905)

References:

[1] N.Y. Abu-Thabit, A.S.H. Makhlouf, Chapter 24 - Recent Advances in Nanocomposite Coatings for Corrosion Protection Applications, in: A.S.H. Makhlouf, D. Scharnweber (Eds.) Handbook of Nanoceramic and Nanocomposite Coatings and Materials, Butterworth-Heinemann2015, pp. 515-549.
[2] E.T. Thostenson, Z.F. Ren, T.W. Chou, Advances in the science and technology of carbon nanotubes and their composites: a review, Compos Sci Technol, 61 (2001) 1899-1912.
[3] F. Kilic, H. Gul, S. Aslan, A. Alp, H. Akbulut, Effect of CTAB concentration in the electrolyte on the tribological properties of nanoparticle SiC reinforced Ni metal matrix composite (MMC) coatings produced by electrodeposition, Colloid Surface A, 419 (2013) 53-60.
[4] V. Braic, A.C. Parau, I. Pana, M. Braic, M. Balaceanu, Effects of substrate temperature and carbon content on the structure and properties of (CrCuNbTiY) C multicomponent coatings, Surf Coat Tech, 258 (2014) 996-1005.
[5] H. Kinoshita, I. Ippei, H. Sakai, N. Ohmae, Synthesis and mechanical properties carbon nanotube/diamond-like carbon composite films, Diam Relat Mater, 16 (2007) 1940-1944.
[6] D. Varshney, A.V. Sumant, B.R. Weiner, G. Morell, Growth of carbon nanotubes on spontaneously detached free standing diamond films and their field emission properties, Diam Relat Mater, 30 (2012) 42-47.

[7] H.Y. Hu, G. Chen, J.Y. Zha, Facile synthesis of CNTs-doped diamond-like carbon film by electrodeposition, Surf Coat Tech, 202 (2008) 5943-5946.
[8] Y. Wang, J.W. Lee, J.G. Duh, Mechanical strengthening in self-lubricating CrAlN/VN multilayer coatings for improved high-temperature tribological characteristics, Surf Coat Tech, 303 (2016) 12-17.
[9] M.I. Yousaf, V.O. Pelenovich, B. Yang, C. Liu, D.J. Fu, Effect of bilayer period on structural and mechanical properties of nanocomposite TiAlN/MoN multilayer films synthesized by cathodic arc ion-plating, Surf Coat Tech, 282 (2015) 94-102.
[10] J. Musil, Hard nanocomposite coatings: Thermal stability, oxidation resistance and toughness, Surf Coat Tech, 207 (2012) 50-65.
[11] L.C. Feng, N. Xie, J. Zhong, Carbon Nanofibers and Their Composites: A Review of Synthesizing, Properties and Applications, Materials, 7 (2014) 3919-3945.
[12] E.T. Thostenson, T.W. Chou, Aligned multi-walled carbon nanotube-reinforced composites: processing and mechanical characterization, J Phys D Appl Phys, 35 (2002) L77-L80.
[13] N. Saba, F. Mohammad, M. Pervaiz, M. Jawaid, O.Y. Alothman, M. Sain, Mechanical, morphological and structural properties of cellulose nanofibers reinforced epoxy composites, Int J Biol Macromol, 97 (2017) 190-200.
[14] S. Iijima, Helical Microtubules of Graphitic Carbon, Nature, 354 (1991) 56-58.
[15] M. Alishahi, S.M. Monirvaghefi, A. Saatchi, S.M. Hosseini, The effect of carbon nanotubes on the corrosion and tribological behavior of electroless Ni–P–CNT composite coating, Appl Surf Sci, 258 (2012) 2439-2446.
[16] K. Han, Z. Liu, H. Ye, F. Dai, Flexible self-standing graphene–Se@CNT composite film as a binder-free cathode for rechargeable Li–Se batteries, J Power Sources, 263 (2014) 85-89.
[17] C. Ma, W. Zhang, Y.-S. He, Q. Gong, H. Che, Z.-F. Ma, Carbon coated SnO2 nanoparticles anchored on CNT as a superior anode material for lithium-ion batteries, Nanoscale, 8 (2016) 4121-4126.
[18] J. Zhao, F. Du, W. Cui, P. Zhu, X. Zhou, X. Xie, Effect of silica coating thickness on the thermal conductivity of polyurethane/SiO2 coated multiwalled carbon nanotube composites, Composites Part A: Applied Science and Manufacturing, 58 (2014) 1-6.
[19] H.W. Zhou, L. Mishnaevsky, H.Y. Yi, Y.Q. Liu, X. Hu, A. Warrier, G.M. Dai, Carbon fiber/carbon nanotube reinforced hierarchical composites: Effect of CNT distribution on shearing strength, Compos Part B-Eng, 88 (2016) 201-211.
[20] C. Guo, Y. Zuo, X.H. Zhao, J.M. Zhao, J.P. Xiong, The effects of electrodeposition current density on properties of Ni-CNTs composite coatings, Surf Coat Tech, 202 (2008) 3246-3250.
[21] C. Guo, Y. Zuo, X.H. Zhao, J.M. Zhao, J.P. Xiong, Effects of surfactants on electrodeposition of nickel-carbon nanotubes composite coatings, Surf Coat Tech, 202 (2008) 3385-3390.
[22] T. He, Y. He, H. Li, Y. Fan, Q.B. Yang, Z. He, A comparative study of effect of mechanical and ultrasound agitation on the properties of pulse electrodeposited Ni-W/MWCNTs composite coatings, J Alloy Compd, 743 (2018) 63-72.
[23] X.H. Chen, C.S. Chen, H.N. Xiao, F.Q. Cheng, G. Zhan, G.J. Yi, Corrosion behavior of carbon nanotubes - Ni composite coating, Surf Coat Tech, 191 (2005) 351-356.
[24] D.G. Liu, J. Sun, Z.X. Gui, K.J. Song, L.M. Luo, Y.C. Wu, Super-low friction nickel based carbon nanotube composite coating electro-deposited from eutectic solvents, Diam Relat Mater, 74 (2017) 229-232.
[25] S. Arai, T. Osaki, M. Hirota, M. Uejima, Fabrication of copper/single-walled carbon nanotube composite film with homogeneously dispersed nanotubes by electroless deposition, Mater Today Commun, 7 (2016) 101-107.

[26] A. Akyol, H. Algul, M. Uysal, H. Akbulut, A. Alp, A novel approach for wear and corrosion resistance in the electroless Ni-P-W alloy with CNFs co-depositions, Appl Surf Sci, 453 (2018) 482-492.
[27] D. Zhang, X. Cui, G. Jin, Z. Cai, B. Lu, Microstructure and mechanical properties of electro-brush plated Fe/MWCNTs composite coatings, Surface and Coatings Technology, 348 (2018) 97-103.
[28] S.R. Bakshi, D. Lahiri, A. Agarwal, Carbon nanotube reinforced metal matrix composites - a review, Int Mater Rev, 55 (2010) 41-64.
[29] S.R. Bakshi, V. Singh, K. Balani, D.G. McCartney, S. Seal, A. Agarwal, Carbon nanotube reinforced aluminum composite coating via cold spraying, Surf Coat Tech, 202 (2008) 5162-5169.
[30] E.J.T. Pialago, C.W. Park, Cold spray deposition characteristics of mechanically alloyed Cu-CNT composite powders, Appl Surf Sci, 308 (2014) 63-74.
[31] H.D. Wang, P.F. He, G.Z. Ma, B.S. Xu, Z.G. Xing, S.Y. Chen, Z. Liu, Y.W. Wang, Tribological behavior of plasma sprayed carbon nanotubes reinforced TiO2 coatings, J Eur Ceram Soc, 38 (2018) 3660-3672.
[32] A.M.K. Esawi, K. Morsi, A. Sayed, M. Tahera, S. Lanka, Effect of carbon nanotube (CNT) content on the mechanical properties of CNT-reinforced aluminium composites, Compos Sci Technol, 70 (2010) 2237-2241.
[33] D. Kaewsai, A. Watcharapasorn, P. Singjai, S. Wirojanupatump, P. Niranatlumpong, S. Jiansirisomboon, Thermal sprayed stainless steel/carbon nanotube composite coatings, Surf Coat Tech, 205 (2010) 2104-2112.
[34] A.K. Keshri, J. Huang, V. Singh, W.B. Choi, S. Seal, A. Agarwal, Synthesis of aluminum oxide coating with carbon nanotube reinforcement produced by chemical vapor deposition for improved fracture and wear resistance, Carbon, 48 (2010) 431-442.
[35] P.H. Jampani, O. Velikokhatnyi, K. Kadakia, D.H. Hong, S.S. Damle, J.A. Poston, A. Manivannan, P.N. Kumta, High energy density titanium doped-vanadium oxide-vertically aligned CNT composite electrodes for supercapacitor applications, J Mater Chem A, 3 (2015) 8413-8432.
[36] H. Zanin, P.W. May, M.H.M.O. Hamanaka, E.J. Corat, Field Emission from Hybrid Diamond-like Carbon and Carbon Nanotube Composite Structures, Acs Appl Mater Inter, 5 (2013) 12238-12243.
[37] R.A. Susantyoko, X.H. Wang, Q.Z. Xiao, E. Fitzgerald, Q. Zhang, Sputtered nickel oxide on vertically-aligned multiwall carbon nanotube arrays for lithium-ion batteries, Carbon, 68 (2014) 619-627.
[38] L. Zhang, B. Zhao, X.Y. Wang, Y.X. Liang, H.X. Qiu, G.P. Zheng, J.H. Yang, Gas transport in vertically-aligned carbon nanotube/parylene composite membranes, Carbon, 66 (2014) 11-17.
[39] S. Vaddiraju, H. Cebeci, K.K. Gleason, B.L. Wardle, Hierarchical Multifunctional Composites by Conformally Coating Aligned Carbon Nanotube Arrays with Conducting Polymer, Acs Appl Mater Inter, 1 (2009) 2565-2572.
[40] H. Zanin, P.W. May, R.L. Harniman, T. Risbridger, E.J. Corat, D.J. Fermin, High surface area diamond-like carbon electrodes grown on vertically aligned carbon nanotubes, Carbon, 82 (2015) 288-296.
[41] X.C. Ji, W. Zhang, X.Y. Li, H.L. Yu, H.S. Dong, A novel hybrid method combining ASP with PECVD for in-situ low temperature synthesis of vertically aligned carbon nanotube films, Diam Relat Mater, 77 (2017) 16-24.
[42] A.L. Del Vecchio, F. Spaepen, The effect of deposition rate on the intrinsic stress in copper and silver thin films, J Appl Phys, 101 (2007).
[43] V. Jourdain, C. Bichara, Current understanding of the growth of carbon nanotubes in catalytic chemical vapour deposition, Carbon, 58 (2013) 2-39.

[44] S.S. Fan, M.G. Chapline, N.R. Franklin, T.W. Tombler, A.M. Cassell, H.J. Dai, Self-oriented regular arrays of carbon nanotubes and their field emission properties, Science, 283 (1999) 512-514.
[45] H. Liu, S.H. Li, J. Zhai, H.J. Li, Q.S. Zheng, L. Jiang, D.B. Zhu, Self-assembly of large-scale micropatterns on aligned carbon nanotube films, Angew Chem Int Edit, 43 (2004) 1146-1149.
[46] Z.F. Ren, Z.P. Huang, J.W. Xu, J.H. Wang, P. Bush, M.P. Siegal, P.N. Provencio, Synthesis of large arrays of well-aligned carbon nanotubes on glass, Science, 282 (1998) 1105-1107.
[47] E. Mosquera, D.E. Diaz-Droguett, N. Carvajal, M. Roble, M. Morel, R. Espinoza, Characterization and hydrogen storage in multi-walled carbon nanotubes grown by aerosol-assisted CVD method, Diam Relat Mater, 43 (2014) 66-71.
[48] R. Saito, M. Hofmann, G. Dresselhaus, A. Jorio, M.S. Dresselhaus, Raman spectroscopy of graphene and carbon nanotubes, Adv Phys, 60 (2011) 413-550.
[49] I. Taurino, S. Carrara, M. Giorcelli, A. Tagliaferro, G. De Micheli, Comparison of two different carbon nanotube-based surfaces with respect to potassium ferricyanide electrochemistry, Surf Sci, 606 (2012) 156-160.
[50] G.H. Jeong, N. Olofsson, L.K.L. Falk, E.E.B. Campbell, Effect of catalyst pattern geometry on the growth of vertically aligned carbon nanotube arrays, Carbon, 47 (2009) 696-704.
[51] Q. Cao, H.S. Kim, N. Pimparkar, J.P. Kulkarni, C.J. Wang, M. Shim, K. Roy, M.A. Alam, J.A. Rogers, Medium-scale carbon nanotube thin-film integrated circuits on flexible plastic substrates, Nature, 454 (2008) 495-U494.
[52] Y.Y. Wei, G. Eres, V.I. Merkulov, D.H. Lowndes, Effect of catalyst film thickness on carbon nanotube growth by selective area chemical vapor deposition, Appl Phys Lett, 78 (2001) 1394-1396.
[53] S. Hofmann, M. Cantoro, B. Kleinsorge, C. Casiraghi, A. Parvez, J. Robertson, C. Ducati, Effects of catalyst film thickness on plasma-enhanced carbon nanotube growth, J Appl Phys, 98 (2005).
[54] A. Lekawa-Raus, J. Patmore, L. Kurzepa, J. Bulmer, K. Koziol, Electrical Properties of Carbon Nanotube Based Fibers and Their Future Use in Electrical Wiring, Adv Funct Mater, 24 (2014) 3661-3682.